IEEE Photonics Journal
An IEEE Photonics Society Publication

Silicon-on-Nitride Waveguide With Ultralow Dispersion Over an Octave-Spanning Mid-Infrared Wavelength Range

Volume 4, Number 1, February 2012

Yang Yue, Student Member, IEEE
Lin Zhang, Student Member, IEEE
Hao Huang, Student Member, IEEE
Raymond G. Beausoleil, Senior Member, IEEE
Alan E. Willner, Fellow, IEEE

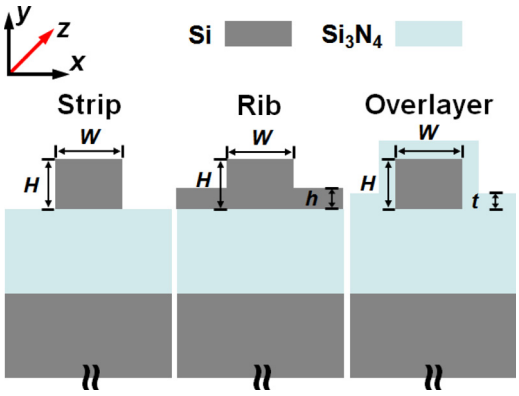

DOI: 10.1109/JPHOT.2011.2180016
1943-0655/$26.00 ©2011 IEEE

Silicon-on-Nitride Waveguide With Ultralow Dispersion Over an Octave-Spanning Mid-Infrared Wavelength Range

Yang Yue,[1] ***Student Member, IEEE*****, Lin Zhang,**[1] ***Student Member, IEEE*****,**
Hao Huang,[1] ***Student Member, IEEE*****,**
Raymond G. Beausoleil,[2] ***Senior Member, IEEE*****, and**
Alan E. Willner,[1] ***Fellow, IEEE***

[1]Department of Electrical Engineering, University of Southern California, Los Angeles, CA 90089 USA
[2]HP Laboratories, Palo Alto, CA 94304 USA

DOI: 10.1109/JPHOT.2011.2180016
1943-0655/$26.00 ©2011 IEEE

Manuscript received November 3, 2011; revised December 5, 2011; accepted December 11, 2011. Date of publication December 15, 2011; date of current version January 6, 2012. This work was supported by HP Laboratories Innovation Research Awards. Corresponding author: Y. Yue (e-mail: yyue@usc.edu).

Abstract: The proposed silicon-on-nitride (SON) waveguide exhibits an ultrabroadband ($\sim$4200 nm), low chromatic dispersion (± 50 ps/(nm $\cdot$ km)) in the mid-infrared (MIR) wavelength region from 2430 to 6630 nm. It has two zero-dispersion wavelengths within the span. Even at 6 μm, the nonlinear coefficients of the SON waveguides are still comparable with the ones of integrated Si_3N_4 waveguides around 1550 nm, which are widely used for octave-spanning nonlinear process. This enables a potential nonlinear optical platform for broadband signal processing across the over-one-octave MIR bandwidth.

Index Terms: Microoptics, optics, subwavelength structures, waveguides.

1. Introduction

Recently, silicon photonics has attracted a lot of attention due to its great potential for complementary metal–oxide semiconductor compatibility [1]. The band gap energy of silicon crystal is close to 1.11 eV. This brings the two-photon absorption (TPA) wavelength range of silicon devices into $\sim$1.1 to 2.2 μm, which covers the widely used telecom band. TPA, which saturates the output power, is one of the critical barriers of silicon waveguides, especially for nonlinear optical signal processing. The free carrier generated by TPA can further distort the signal [2], [3]. By incorporating an integrated p-i-n diode with reverse bias, the carriers can be efficiently extracted [4]–[6].

The mid-infrared (MIR) wavelength region, which covers 3 to 8 μm [7], is of great interest for several applications, such as astronomy, chemical bond spectroscopy, environmental monitoring, free-space communication, optical sensing, and thermal imaging [8]–[10]. Integrating active and passive components to form an on-chip photonic circuit is a laudable goal to compact the MIR system, of which the waveguide is the basic building block [8], [9]. The lack of TPA of silicon in the MIR provides great potential for nonlinear optics using silicon waveguides [11]–[15]. Over the past few years, Si waveguides and devices for MIR have been developed for different applications [16]–[22]. Moreover, on-chip silicon waveguides for long wavelength applications are relatively large in size and thus yield the fabrication accuracy required to achieve desired properties.

Broadband low dispersion, high nonlinearity and low loss are desirable goals for many broadband nonlinear signal processing applications, such as broadband wavelength conversion, supercontinuum generation and frequency comb generation [14], [23]–[25]. Operating at MIR can

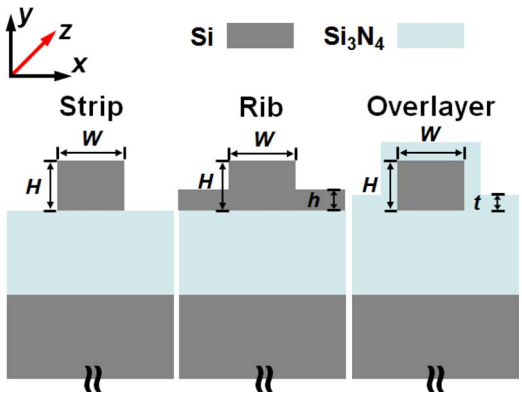

Fig. 1. Cross sections of strip, rib, and conformal overlayer SON waveguides.

pronouncedly reduce the nonlinear loss, while the waveguide materials should be chosen properly to reduce the material absorption induced linear loss. Silicon dioxide is lossy at wavelengths from 2.6 to 2.9 μm and beyond 3.6 μm, and thus becomes improper for MIR applications. Silicon-on-sapphire waveguides can extend the low-loss wavelength of substrate material to $\sim$4.5 μm [9]. It also shows the potential to achieve small dispersion $(\pm 50\ \text{ps}/(\text{nm}\cdot\text{km}))$ over $\sim$1700-nm bandwidth, which is up to $\sim$4 μm [21]. As a complementary metal–oxide–semiconductor process compatible platform, silicon nitride waveguides and devices have shown efficient nonlinear effects over octave bandwidth range [23], [25]. Promisingly, silicon nitride also has higher nonlinear refractive index [26], [27] and remains low loss for wavelengths from 1.2 to 6.6 μm, which can better match the broader low-loss wavelength range of Si (up to $\sim$8.5 μm) [9]. Thus, the MIR silicon-on-nitride (SON) waveguide has the great potential to achieve these features [8], [9].

In this paper, we engineer and flatten the chromatic dispersion of strip, rib and conformal overlayer SON waveguide in the MIR wavelength region. The rib and conformal overlayer waveguides provide more structural parameters to tailor the chromatic dispersion for broadband low-dispersion operation. A low dispersion of $\pm$50-ps$/(\text{nm}\cdot\text{km})$ is achieved over a 4200-nm bandwidth from 2430 to 6630 nm using the SON rib waveguide. With a proper design, two zero-dispersion wavelengths (ZDWs) can be obtained beyond the TPA wavelength edge. Moreover, a relatively large nonlinear coefficient can potentially enable nonlinear process, such as supercontinuum and frequency comb generation, across the over-one-octave bandwidth.

2. Waveguide Structure and Mode Property

The cross sections of strip, rib, and conformal overlayer SON waveguides are shown in Fig. 1, where W, H, h, and t represent the waveguide width, waveguide height, slab height, and overlayer thickness, respectively. The gray regions are silicon, and the blue regions are silicon nitride. There is a 2-μm silicon nitride space layer on the Si substrate. The material refractive indices of silicon and silicon nitride are obtained according to the Sellmeier equations [28], [29] in our model. In the simulation, the dispersion of nonlinear refractive index (n_2) for silicon is considered [21]. We develop a 8×8 μm^2 model using a full-vector finite-element method (COMSOL). A convergence test shows a 2-μm Si substrate and 1-μm perfectly matched layer can provide accurate results. We obtain the effective refractive indices and mode distributions of the eigenmodes for SON waveguides with different structural parameters over a broad spectral range. Chromatic dispersions are obtained by taking the second-order derivatives of the effective refractive indices, and nonlinear coefficients (γ) are calculated from the mode distributions using a full-vector model [30].

To achieve good light confinement over a broad bandwidth that expands to MIR, we use waveguide sizes that are larger than single-mode waveguides for communication band around 1.55 μm. Here, we study the modal characteristics of SON waveguides. Fig. 2(a) shows the dispersion property of the conformal overlayer SON waveguide $(W = 2000\ \text{nm}, H = 800\ \text{nm}, t = 400\ \text{nm})$. TE_{11} and TM_{11} are

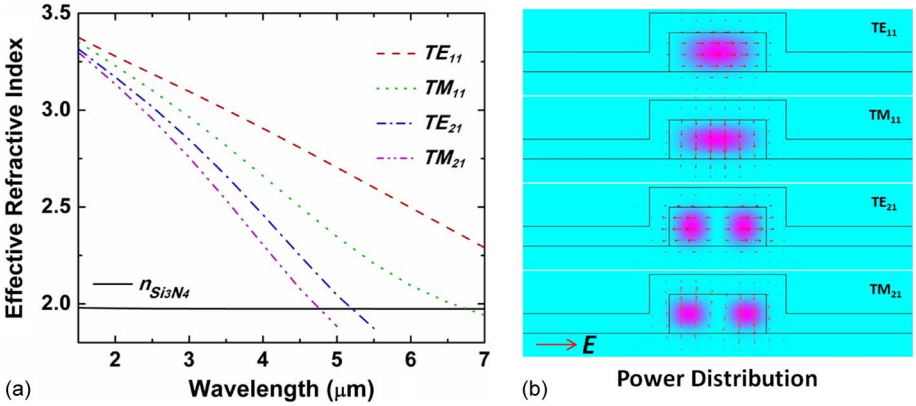

Fig. 2. (a) Dispersion property and (b) power distribution (3 μm) of the conformal overlayer SON waveguide ($W = 2000$ nm, $H = 800$ nm, $t = 400$ nm) modes.

the x- and y- polarized fundamental modes, while TE_{21} and TM_{21} are the second-order modes with x- and y- polarizations. At 3 μm, as shown in Fig. 2(b), the modes are well confined within the silicon core region. At short wavelengths, the effective refractive indices are close to the material index of Si, and the index difference between the fundamental and higher order modes is small. The effective refractive indices decrease with wavelength, while the index difference increases. Moreover, the effective refractive indices of higher order modes approach the material index of Si_3N_4 more quickly. In such case, the higher order modes leaks out much more quickly than the fundamental modes at the long wavelength range. At 5.19 μm, all higher order modes are cut off, and the x-polarized fundamental mode is still well guided ($n_{TE11} = 2.64$). The single-mode operational wavelength region can be blue shifted by reducing the waveguide size. In general, the propagation loss increases with wavelength due to the reduced confinement and more interaction with the rough sidewalls. With a good fabrication process, 1–2 dB/cm propagation loss can be potentially achieved at long wavelength region [22].

3. Chromatic Dispersion

In general, chromatic dispersion stems from two sources: material dispersion and waveguide dispersion. In the long-wavelength region (> 3 μm), silicon and silicon nitride have small negative material dispersions. This is because this region is far away from their band-gap wavelengths. Consequently, waveguide dispersion dominates in the total dispersion. A large waveguide not only provides good light confinement but reduces the waveguide dispersion as well.

Fig. 3(a) shows the chromatic dispersions of x-polarized fundamental mode in a strip SON waveguide with different H. The height of the strip waveguide decreases from 1400 to 600 nm, while its width remains the same (2000 nm). For the low height waveguide, the mode is confined more tightly and experiences more waveguide dispersion. Thus, the chromatic dispersion starts to decrease at a relatively shorter wavelength. A strip SON waveguide with a 2000-nm width and a 600-nm height exhibits a dispersion of ± 150 ps/(nm $\cdot$ km) over 3350-nm bandwidth from 1840 to 5190 nm. The effect of strip waveguide height on the chromatic dispersions of y-polarized fundamental mode is shown in Fig. 3(b). Compared with the dispersion of x-polarized mode, the impact of waveguide height on the dispersion of y-polarized mode is more pronounced. The chromatic dispersion reaches its maximum 536 ps/(nm $\cdot$ km) at 5630 nm for $H = 1600$ nm. For $H = 800$ nm, the maximum chromatic dispersion is 766 ps/(nm $\cdot$ km) at 3040 nm.

Fig. 4 shows the chromatic dispersions of x- and y-polarized fundamental modes in strip SON waveguides with different W. The height of the strip waveguide remains as 1200 nm, while its width increases from 1600 to 3200 nm. With the increasing waveguide width, the x-polarized mode has a released confinement. Both the value and slope of its chromatic dispersion decrease. A strip SON waveguide with 3200-nm width and 1200-nm height has a dispersion of 200 ps/(nm $\cdot$ km) over the

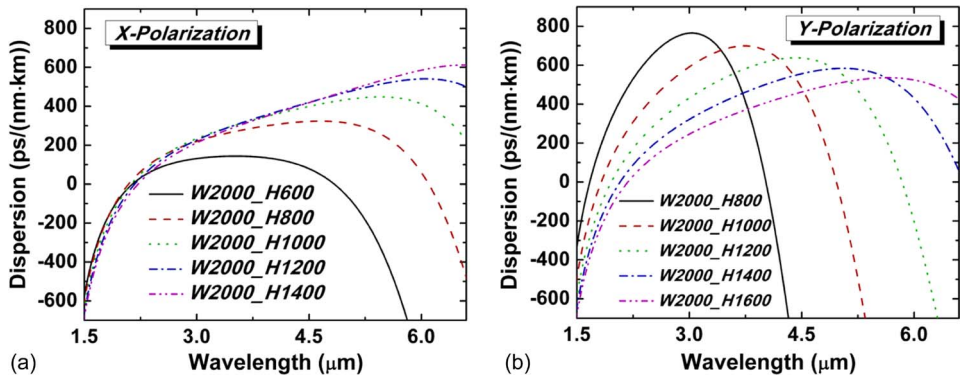

Fig. 3. Chromatic dispersion of (a) *x*- and (b) *y*-polarized fundamental modes for strip SON waveguide with different waveguide height.

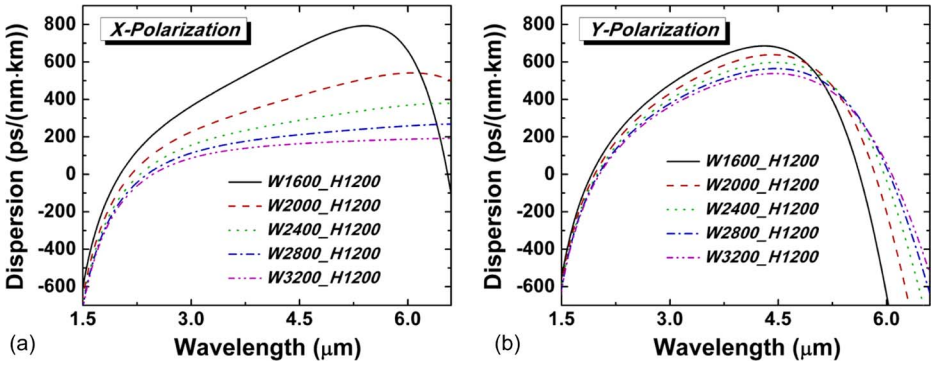

Fig. 4. Chromatic dispersion of (a) *x*- and (b) *y*-polarized fundamental modes for strip SON waveguide with different waveguide widths.

5000-nm bandwidth. The impact of waveguide width on the chromatic dispersion for *y*-polarized fundamental modes is small due to the fixed structure parameter in *y*-dimension (H).

The rib waveguide can be fabricated by underetching the high-index guiding layer as illustrated in Fig. 1. The chromatic dispersion of the fundamental mode in *x*-polarization as a function of the wavelength in the rib SON waveguide is shown in Fig. 5(a). Rib height (H) is 1200 nm, and rib width (W) is 2000 nm. The slab height (h) of the rib waveguide increases from 0 to 1000 nm. The increase of slab height gives more space for the mode to extend and thus yields a lower chromatic dispersion. With the increase of slab height (h) from 0 to 1000 nm, the chromatic dispersion decreases from 500 to 50 ps/(nm · km) over an ultrawide bandwidth. The rib waveguide with a 1000-nm slab height exhibits a ± 50 ps$/(\text{nm} \cdot \text{km})$ dispersion with a 4200-nm bandwidth from 2430 to 6630 nm.

As shown in Fig. 1, the conformal overlayer waveguide can be realized by depositing another low-index layer of silicon nitride film on the strip waveguide [31]. The chromatic dispersion of the fundamental mode for *x*-polarization in the conformal overlayer SON waveguide $(W = 2000 \text{ nm}, H = 800 \text{ nm})$ is shown in Fig. 5(b). The thickness of the overlayer (t) increases from 0 to 800 with a step of 200 nm. The additional low-index overlayer surrounding the high-index silicon guiding core can be used to control the balance between material and waveguide dispersion, producing the desired net dispersion characteristics. Compared between $t = 0$ and 800 nm, not only the value but also the slope polarity of the chromatic dispersion are tuned. The conformal overlayer waveguide with an 800-nm overlayer has a 3740-nm bandwidth for chromatic dispersion within ± 120 ps$/(\text{nm} \cdot \text{km})$.

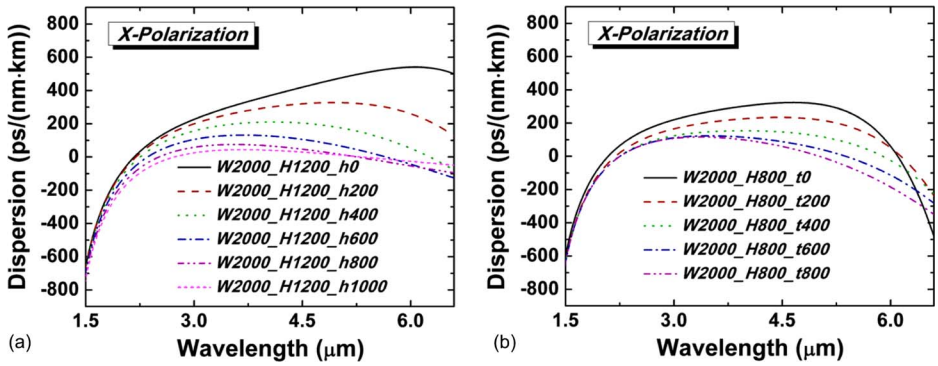

Fig. 5. Chromatic dispersion of *x*-polarized fundamental modes for (a) rib SON waveguide with different slab height and (b) conformal overlayer SON waveguide with different overlayer thickness.

TABLE 1

Zero-dispersion wavelength in the conformal overlayer waveguides

Structure Parameters (W×H_t) (nm)	ZDW_1 (nm)	ZDW_2 (nm)
2000×800_0	2090	6097
2000×800_200	2193	6142
2000×800_400	2243	5885
2000×800_600	2250	5380
2000×800_800	2258	5014

ZDWs are critical to achieve the phase matching condition, especially for nonlinear four-wave mixing (FWM) process. Table 1 shows the ZDWs in the dispersion curves of the *x*-polarized fundamental modes for conformal overlayer SON waveguides. There are two ZDWs for different t from 0 to 800 nm. First, ZDW_1 is around the TPA edge of Si (2200 nm), and thus, the waveguide have pronouncedly reduced nonlinear absorption by operating around this ZDW. Second, ZDW_2, which is above 5 μm, can efficiently bring the nonlinear parametric wavelength conversion to a longer wavelength range. With proper design, two ZDWs can also be achieved in strip and rib SON waveguides between 2 and 6 μm.

4. Nonlinearity

For the nonlinear FWM process, the ultrabroadband low dispersion waveguide facilitates the phase matching for different signals over a broad wavelength range. Another parameter that affects the efficiency of the parametric wavelength conversion is the nonlinearity of the waveguide. To take the wavelength dependence of material's nonlinear response into account, the dispersion of n_2 for silicon is considered, as shown in Fig. 6(a) [21]. In the simulation, the nonlinear refractive indices n_2 for Si_3N_4 is 2.4×10^{-19} m^2/W [26]. As the bandgap wavelengths of Si_3N_4 is below 245 nm, the change of its nonlinear refractive index at wavelength beyond 1.5 μm is small. Moreover, because most of the modal field is confined within silicon, the impact from the dispersion of nonlinear refractive indices for Si_3N_4 to the total waveguide nonlinearity further decreases. Fig. 6(b) shows the nonlinear coefficients of strip ($W = 2000$ nm, $H = 600$ nm), rib ($W = 2000$ nm, $H = 1200$ nm, $h = 600$ nm), and conformal overlayer ($W = 2000$ nm, $H = 800$ nm, $t = 400$ nm) SON waveguides. For ± 150 ps/(nm · km) chromatic dispersion, strip, rib and conformal overlayer waveguide have 3350-nm, 4800-nm, and 3510-nm bandwidths, respectively. From Fig. 6(b), we can see that the strip waveguide has the largest nonlinear coefficient at a short wavelength ($\gamma = 8.32$ /W/m @ 3 μm) for up to 6 μm and that its nonlinearity decreases fastest. This is because the strip waveguide has the smallest cross section

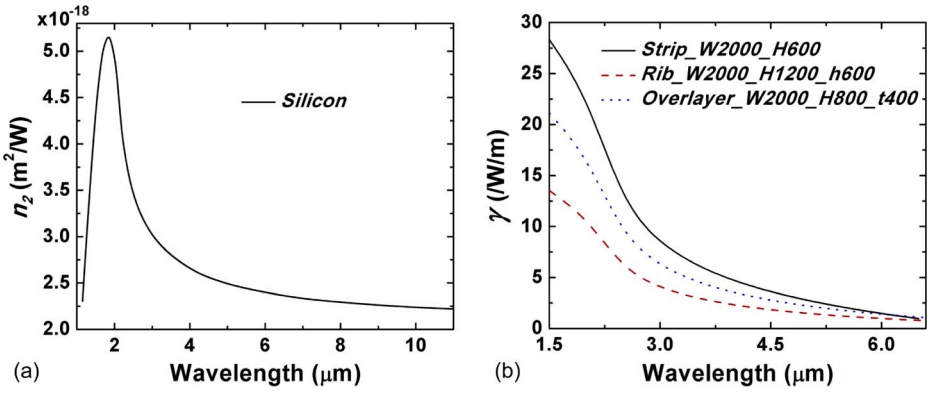

Fig. 6. (a) Nonlinear refractive index of silicon and (b) the nonlinear coefficients in strip, rib, and conformal overlayer waveguides.

among these three waveguides. Therefore, it provides a tighter light confinement and gives a smaller mode area at a short wavelength. At longer wavelengths, the strip waveguide is too small to provide good confinement, while the size of rib and conformal overlayer waveguides are still large enough. Moreover, the rib and conformal overlayer waveguides provide more waveguide parameters to engineer chromatic dispersion for broadening low-dispersion bandwidth and enhance the mode confinement while maintaining comparable nonlinearity in the long wavelength region. Even at a long wavelength range around 6 μm, the nonlinear coefficients of SON waveguides ($\gamma = 1.46$ /W/m) are still comparable with the ones of integrated Si_3N_4 waveguides around 1.55 μm, which are widely used for octave-spanning nonlinear process [23], [25]. Because of the reduced nonlinear coefficient and potentially increased propagation loss, the efficiency of the nonlinear process is expected to be lower at longer wavelength.

5. Conclusion

With proper design, over-one-octave broadband ultralow chromatic dispersion is achieved using SON waveguide in MIR wavelength region. From 2430 to 6630 nm, a $\pm$50-ps/(nm $\cdot$ km) chromatic dispersion is achieved over a 4200-nm bandwidth using the rib SON waveguide. Two ZDWs, which are beyond the TPA wavelength edge, can be obtained with strip, rib, and conformal overlayer SON waveguides. Together with relatively large nonlinear coefficients, they offer great potential to achieve wavelength conversion, supercontinuum generation, and frequency comb generation over-one-octave bandwidth.

References

[1] L. Pavesi and G. Guillot, *Optical Interconnects: The Silicon Approach*. Heidelberg, Germany: Springer-Verlag, 2006.
[2] Q. Lin, J. Zhang, G. Piredda, R. W. Boyd, P. M. Fauchet, and G. P. Agrawal, "Dispersion of silicon nonlinearities in the near-infrared region," *Appl. Phys. Lett.*, vol. 91, no. 2, p. 021111, Jul. 2007.
[3] Q. Lin, O. J. Painter, and G. P. Agrawal, "Nonlinear optical phenomena in silicon waveguides: Modeling and applications," *Opt. Exp.*, vol. 15, no. 25, pp. 16 604–16 644, Dec. 2007.
[4] H. Rong, Y.-H. Kuo, A. Liu, M. Paniccia, and O. Cohen, "High efficiency wavelength conversion of 10 Gb/s data in silicon waveguides," *Opt. Exp.*, vol. 14, no. 3, pp. 1182–1188, Feb. 2006.
[5] A. C. Turner-Foster, M. A. Foster, A. L. Gaeta, and M. Lipson, "Large Enhancement of Wavelength Conversion in Silicon Nanowaveguides via Free-Carrier Removal," in *Conf. Lasers Electro-Optics, OSA Tech. Dig.*, San Jose, CA, 2010, Paper CTuEE1.
[6] J. Cardenas, J. S. Levy, G. Weiderhecker, A. Turner-Foster, A. L. Gaeta, and M. Lipson, "Efficient frequency conversion at low-powers in a silicon microresonator using carrier extraction," in *CLEO-Laser Appl. Photon. Appl., OSA Tech. Dig.*, Baltimore, MD, 2011, Paper CTuX2.
[7] J. Byrnes, *Unexploded Ordnance Detection and Mitigation*. Amsterdam, The Netherlands: Springer-Verlag, 2009.
[8] R. A. Soref, S. J. Emelett, and A. R. Buchwald, "Silicon waveguided components for the long-wave infrared region," *J. Opt. A, Pure Appl. Opt.*, vol. 8, no. 10, pp. 840–848, 2006.
[9] R. Soref, "Mid-infrared photonics in silicon and germanium," *Nat. Photon.*, vol. 4, no. 8, pp. 495–497, 2010.

[10] M. Ebrahim-Zadeh and I. T. Sorokina, *Mid-Infrared Coherent Sources and Applications*. New York: Springer-Verlag, 2007.
[11] V. Raghunathan, D. Borlaug, R. R. Rice, and B. Jalali, "Demonstration of a mid-infrared silicon Raman amplifier," *Opt. Exp.*, vol. 15, no. 22, pp. 14 355–14 362, Oct. 2007.
[12] X. P. Liu, R. M. Osgood, Y. A. Vlasov, and W. M. J. Green, "Mid-infrared optical parametric amplifier using silicon nanophotonic waveguides," *Nat. Photon.*, vol. 4, pp. 557–560, 2010.
[13] X. P. Liu, J. B. Driscoll, J. I. Dadap, R. M. Osgood, S. Assefa, Y. A. Vlasov, and W. M. J. Green, "Self-phase modulation and nonlinear loss in silicon nanophotonic wires near the mid-infrared two-photon absorption edge," *Opt. Exp.*, vol. 19, no. 8, pp. 7778–7789, Apr. 2011.
[14] R. K. W. Lau, M. Ménard, Y. Okawachi, M. A. Foster, A. C. Turner-Foster, R. Salem, M. Lipson, and A. L. Gaeta, "Continuous-wave mid-infrared frequency conversion in silicon nanowaveguides," *Opt. Lett.*, vol. 36, no. 7, pp. 1263–1265, Apr. 2011.
[15] S. Zlatanovic, J. S. Park, S. Moro, J. M. C. Boggio, I. B. Divliansky, N. Alic, S. Mookherjea, and S. Radic, "Mid-infrared wavelength conversion in silicon waveguides using ultracompact telecom-band-derived pump source," *Nat. Photon.*, vol. 4, no. 8, pp. 561–564, Aug. 2010.
[16] M. M. Milosevic, P. S. Matavulj, P. Y. Y. Yang, A. Bagolini, and G. Z. Mashanovich, "Rib waveguides for mid-infrared silicon photonics," *J. Opt. Soc. Amer. B-Opt. Phys.*, vol. 26, no. 9, pp. 1760–1766, Sep. 2009.
[17] T. Baehr-Jones, A. Spott, R. Ilic, B. Penkov, W. Asher, and M. Hochberg, "Silicon-on-sapphire integrated waveguides for the mid-infrared," *Opt. Exp.*, vol. 18, no. 12, pp. 12 127–12 135, Jun. 2010.
[18] A. Spott, Y. Liu, T. Baehr-Jones, R. Ilic, and M. Hochberg, "Silicon waveguides and ring resonators at 5.5 μm," *Appl. Phys. Lett.*, vol. 97, no. 21, p. 213501, Nov. 2010.
[19] R. Shankar, R. Leijssen, I. Bulu, and M. Loncar, "Mid-infrared photonic crystal cavities in silicon," *Opt. Exp.*, vol. 19, no. 6, pp. 5579–5586, Mar. 2011.
[20] G. Z. Mashanovich, M. M. Milosevic, M. Nedeljkovic, N. Owens, B. Q. Xiong, E. J. Teo, and Y. F. Hu, "Low loss silicon waveguides for the mid-infrared," *Opt. Exp.*, vol. 19, no. 8, pp. 7112–7119, Apr. 2011.
[21] E. K. Tien, Y. W. Huang, S. M. Gao, Q. Song, F. Qian, S. K. Kalyoncu, and O. Boyraz, "Discrete parametric band conversion in silicon for mid-infrared applications," *Opt. Exp.*, vol. 18, no. 21, pp. 21 981–21 989, Oct. 2010.
[22] F. Li, S. D. Jackson, C. Grillet, E. Magi, D. Hudson, S. J. Madden, Y. Moghe, C. O'Brien, A. Read, S. G. Duvall, P. Atanackovic, B. J. Eggleton, and D. J. Moss, "Low propagation loss silicon-on-sapphire waveguides for the mid-infrared," *Opt. Exp.*, vol. 19, no. 16, pp. 15 212–15 220, Aug. 2011.
[23] L. Zhang, Y. Yan, Y. Yue, Q. Lin, O. Painter, R. G. Beausoleil, and A. E. Willner, "On-chip two-octave supercontinuum generation by enhancing self-steepening of optical pulses," *Opt. Exp.*, vol. 19, no. 12, pp. 11 584–11 590, Jun. 2011.
[24] J. S. Levy, A. Gondarenko, M. A. Foster, A. C. Turner-Foster, A. L. Gaeta, and M. Lipson, "CMOS-compatible multiple-wavelength oscillator for on-chip optical interconnects," *Nat. Photon.*, vol. 4, no. 1, pp. 37–40, Jan. 2010.
[25] Y. Okawachi, K. Saha, J. S. Levy, Y. H. Wen, M. Lipson, and A. L. Gaeta, "Octave-spanning frequency comb generation in a silicon nitride chip," *Opt. Lett.*, vol. 36, no. 17, pp. 3398–3400, Sep. 2011.
[26] K. Ikeda, R. E. Saperstein, N. Alic, and Y. Fainman, "Thermal and Kerr nonlinear properties of plasma-deposited silicon nitride/silicon dioxide waveguides," *Opt. Exp.*, vol. 16, no. 17, pp. 12 987–12 994, Aug. 2008.
[27] A. Major, F. Yoshino, I. Nikolakakos, J. S. Aitchison, and P. W. E. Smith, "Dispersion of the nonlinear refractive index in sapphire," *Opt. Lett.*, vol. 29, no. 6, pp. 602–604, Mar. 2004.
[28] E. D. Palik, *Handbook of Optical Constants of Solids*. San Diego, CA: Academic, 1998.
[29] T. Baak, "Silicon oxynitride; a material for GRIN optics," *Appl. Opt.*, vol. 21, no. 6, pp. 1069–1072, Mar. 1982.
[30] A. V. Shahraam and T. M. Monro, "A full vectorial model for pulse propagation in emerging waveguides with subwavelength structures part I: Kerr nonlinearity," *Opt. Exp.*, vol. 17, no. 4, pp. 2298–2318, Feb. 2009.
[31] X. P. Liu, W. M. J. Green, X. G. Chen, I. W. Hsieh, J. I. Dadap, Y. A. Vlasov, and R. M. Osgood, "Conformal dielectric overlayers for engineering dispersion and effective nonlinearity of silicon nanophotonic wires," *Opt. Lett.*, vol. 33, no. 24, pp. 2889–2891, Dec. 2008.